ELSEVIER

Contents lists available at ScienceDirect

# Journal of Membrane Science

journal homepage: www.elsevier.com/locate/memsci





# Percolation-assisted coating of metal-organic frameworks on porous substrates

Rajan R. Bhawnani <sup>a</sup>, Rohan Sartape <sup>a</sup>, Aditya Prajapati <sup>a</sup>, Prem K.R. Podupu <sup>a</sup>, Paria Coliaie <sup>a</sup>, Arnav N. Nere <sup>b</sup>, Meenesh R. Singh <sup>a</sup>, <sup>\*</sup>

#### ARTICLE INFO

Keywords: Metal-organic framework film Percolation-assisted coating Microfluidic Continuous processing Gas separation

# ABSTRACT

In the past two decades, significant advancements have been made toward thin film fabrication of metal-organic frameworks (MOFs) on porous solid substrates for gas separation and catalysis applications. To enhance the physical and chemical stability of the films, various top-down and bottom-up approaches have been implemented. While both approaches have some advantages, they are mostly limited due to a lack of adhesion with the substrate, cracking of the films, and non-uniform coverages. Therefore, there is a need for improvement in the coating processes for the fabrication of robust, uniform, and scalable films. Here, we develop a novel percolationassisted coating (PAC) process that combines top-down and bottom-up approaches in a continuous-flow microfluidic device to deposit HKUST-1 on a porous substrate, yielding controlled film thicknesses and mass loading. The PAC process is optimized using a Multiphysics modeling approach to design the microfluidic reactor, which can be readily scaled up and deployed to fabricate MOF films on various porous substrates. The desired thickness in the range of 10-200 µm of the MOF film can be achieved by controlling the residence time and temperature of the reaction mixture. The synthesized film is characterized for physical adhesion using sonication, film coverage using scanning electron microscopy, and porosity using a porosimeter. The performance of synthesized films is benchmarked for the effective separation of 50 vol% CH<sub>4</sub>-H<sub>2</sub> gas mixture with the separation factor of 4. The microfluidic device is also applicable to synthesize films of various MOFs like MOF-5, MOF-505 (also reported here), UIO-66, etc., over a wide range of porous substrates. Lastly, we propose a multichamber design of the microfluidic device for high-throughput screening of thin-film growth using the PAC process.

## 1. Introduction

Metal-organic frameworks (MOFs) are a class of hybrid, porous crystalline materials that have gained significant attention in the previous two decades [1,2]. These complex networks are formed by self-assembly and oriented attachment of metallic nodes/ions (mainly transition metals) connected by an organic linker. These periodic networks exhibit large specific surface area, ordered pore diameters, and flexibility for functional group modifications as needed, thus making them a frontrunner in a wide range of applications [3–9]. Numerous studies have demonstrated MOFs like UIO-66, HKUST-1, MIL-53, MOF-5, etc., as excellent candidates in catalysis, gas adsorption and separation, and water purification [3,10–17]. Majority of these applications use these materials as a film/membrane (either free-standing or

deposited on a substrate); thus, it is essential to fabricate uniform and conformally coated MOF films with optimal thickness and mechanical strength [10,14,18–22].

Pure or composite MOF films are deposited on a wide range of substrates (solid and porous) by various solvothermal, electrochemical, and coating techniques [20,21,23–25]. Solvothermally, layer-by-layer (LbL) fabrication of MOFs is one of the primal techniques proposed by Fischer and co. to deposit thin films of MOF-5 on gold substrates utilizing a self-assembled monolayer (SAM) [26,27]. Similar approach was implemented in fabricating HKUST-1 films by Farha and coworkers while also displaying the effect of solvents on the qualitative aspects of the films [27]. [28]. Although several studies claim that this approach yields desired thickness and loading, the approach requires precise control of heterogeneous nucleation to ensure uniform deposition [27,29–31].

<sup>&</sup>lt;sup>a</sup> Department of Chemical Engineering, University of Illinois Chicago, Chicago, IL, 60607, USA

b Vernon Hills High School, Vernon Hills, IL, 60061, USA

<sup>\*</sup> Corresponding author. Department of Chemical Engineering, 929 W. Taylor St, University of Illinois Chicago, Chicago, IL, 60607, USA. E-mail address: mrsingh@uic.edu (M.R. Singh).

This makes the LbL protocol very time and labor-intensive. As an alternative to a bottom-up approach like LbL, where the crystallization is carried out directly on the substrate, researchers have also implemented top-down approaches, in which the crystals are synthesized in batch and then suspended in a liquid matrix to coat them on a substrate [3,18,19, 32]. Coating is carried out in a variety of approaches like spin coating, dip coating, titration coating, etc. [3,32,33] While coating ensures a uniform and conformal deposition, controlling the quantitative aspects of the film such as thickness, grain size distribution, and uniformity, limited scalability of the process and lower adhesion of the deposited material on the substrate have been the primary concerns of this approach [34].

In conjunction with these approaches, continuous processing techniques have also been employed to overcome some of the diffusion limitations and turbulent environments [16–26]. These approaches have allowed significant control over the final attributes like film thickness and grain size distribution of the deposited crystallites. The early-stage continuous microfluidic synthesis of thin films was conducted using hollow fibers to fabricate thin films of ZIF-8 [35]. Along with this approach, nanoconfined channels have been used to fabricate high aspect ratio deposition on the substrates [36]. Supersaturation-induced film deposition is one of the most popular continuous microfluidic techniques, where the reaction between the precursors is induced by vaporizing the solvent via blade shearing [34,37–44].

While these continuous techniques have proven to be effective in improving the final adhesion and minimizing the inter-grain spacing of the films, they have mostly been implemented on solid substrates. In the case of gas separations, pure MOF film depositions are required on a porous membrane while ensuring strong adhesion, minimal grain boundary defects, low inter-grain spacing, and narrow size distribution of the deposited crystallites. Obtaining pure MOF membranes on porous

substrates while ensuring these qualities has been challenging in the topdown and bottom-up approaches mentioned previously due to cracking and weak bonding with the substrates resulting in lower mechanical integrity and many stability concerns [34]. These properties are essential to address for gas separation applications as they determine the selectivity of the transport pathways for gas molecules in binary or ternary mixtures. To overcome these challenges, a novel continuous, in-situ approach is proposed, which involves a coupled seeding (bottom-up approach) and percolation (top-down approach) deposition method, demonstrated on HKUST-1. This technique, coupled with optimal solvent choices and postprocessing procedures, ensures a well-patched, continuous network with conformal material deposition and minimal inter-grain spacing. HKUST-1 has proven to be an excellent candidate for the separation of many binary gas mixtures like CO<sub>2</sub>/N<sub>2</sub>, CO<sub>2</sub>/CH<sub>4</sub>, CH<sub>4</sub>/H<sub>2</sub>, etc. [34] The effectiveness of the fabricated HKUST-1 films in this work has been demonstrated in the separation of CH<sub>4</sub>/H<sub>2</sub> mixture.

Through an in-house 3D printed tubular flow reactor-separator assembly, a well-controlled continuous approach to fabricating films of HKUST-1 with a wide range of thicknesses (20–200  $\mu m$ ) and mass loading (5–50 mg/cm²) is presented. HKUST-1 continuously forms in a tubular chamber, opening into a square chamber where the crystallites are deposited on a porous substrate. The deposition is completely guided by percolation initially. However, as time proceeds, crystals start getting deposited on the substrate, thereby blocking the passage of the reaction effluent partially. This leads to heterogeneous nucleation-induced secondary growth of MOF film. The deposition mechanism is thus driven by a combined percolation-assisted seeded growth. This percolation-assisted coating (PAC) technique ensures the contiguous network of crystallites, thereby minimizing the inter-grain spacing and strengthening the adhesion with the substrate. Once the deposition is complete,

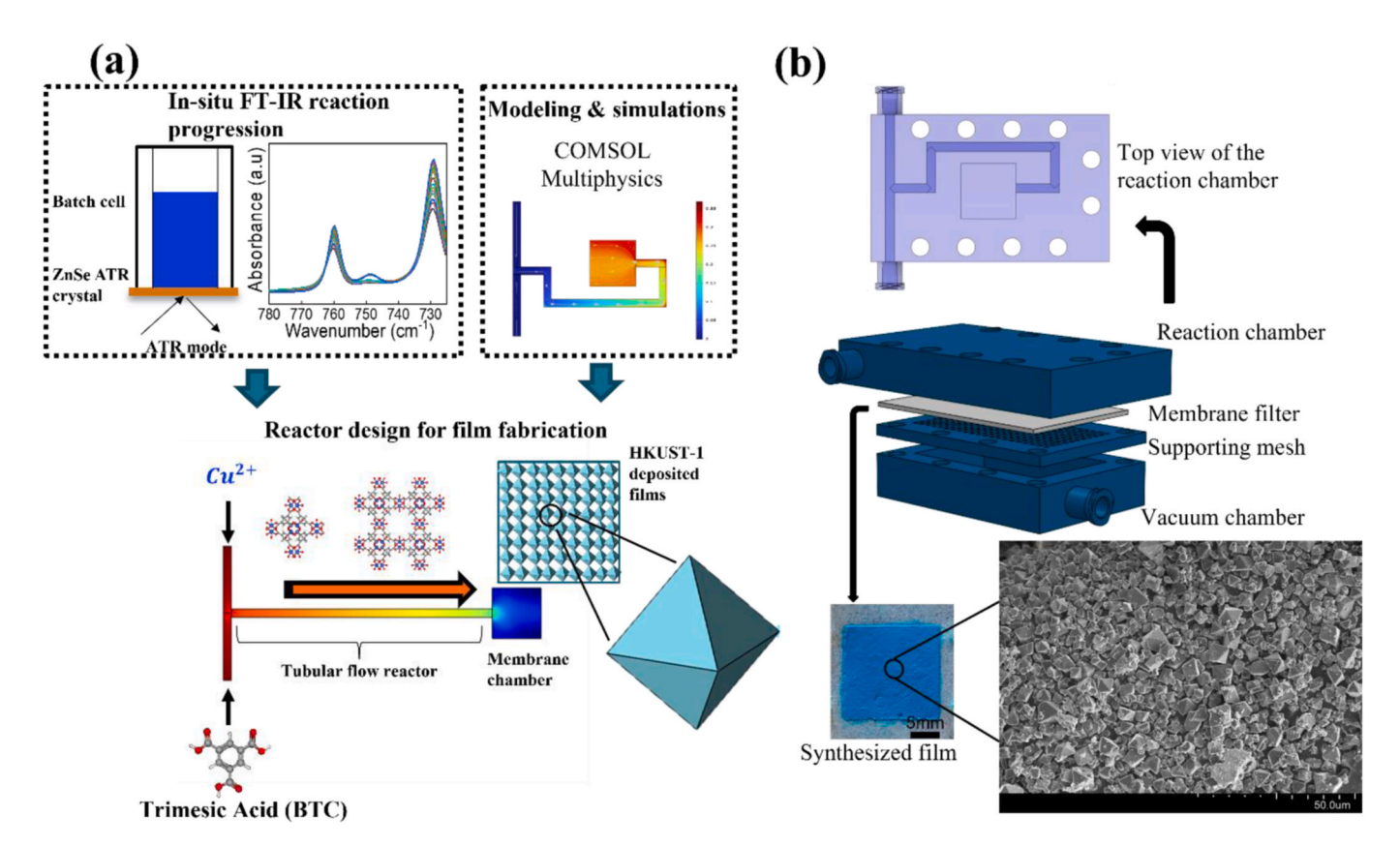


Fig. 1. (a) Overall schematic of fabrication of HKUST-1 films in a reactor-separator assembly using in-situ batch experiments combined with modeling and simulations in COMSOL to design and model a lab-scale tubular flow reactor. (b) Solidworks design (TOP) of the 3D printed tubular reactor-separation chamber (top part), membrane supporting mesh (middle part), and vacuum chamber (bottom part) for solvent separation. Optical image of deposited HKUST-1 (bottom, left) of  $15 \times 15$  mm size on a nylon filter/membrane and the magnified SEM image of the deposited crystals.

vacuum is applied to eliminate the small amounts of reactant effluent trapped in the film/substrate. Fig. 1(a) shows the overall schematic of the workflow. Batch in-situ Fourier Transformed Infrared Spectroscopy (FTIR) experiments are first performed to study the kinetics of HKUST-1 formation for a range of temperatures. The reactive transport in microfluidic channels is then simulated using the measured rate constants in COMSOL Multiphysics to obtain MOF yield and mixing profiles. Scanning Electron Microscopy (SEM) and optical microscopy are used to measure the thicknesses of MOF films. Brunauer-Emmett-Teller (BET) measurements of exfoliated films confirmed the characteristic porosity of HKUST-1. Postprocessing strategies are applied to quantify the mechanical strength and adhesion of the films. Finally, the performance of these films for  $\mathrm{CH_4-H_2}$  separation is demonstrated, where HKUST-1 showed higher selectivity for  $\mathrm{CH_4}$ , similar to what has been observed in previous studies.

# 2. Materials & methods

## 2.1. Materials

0.4~M Copper nitrate trihydrate (Cu(NO<sub>3</sub>)<sub>2</sub> 3H<sub>2</sub>O) and 0.22~M Trimesic acid (BTC) were individually dissolved in Dimethylformamide (DMF) for the synthesis of HKUST-1 in FTIR and film fabrication experiments. Refer section S1 of the supporting information for details.

## 2.2. In-situ kinetic studies using FTIR

The batch kinetics of HKUST-1 formation was studied using in-situ FTIR in ATR mode. An in-house 3D printed cell was mounted on a temperature-controlled ZnSe ATR crystal plate and a total of 1 mL reactant mixture was loaded into the cell. The experiments were performed at different temperatures to obtain the Arrhenius plot that further yields the activation energy value required for COMSOL simulations. The calibration plot of known HKUST-1 concentrations in DMF and experimental setup for in-situ FTIR studies are included in section S2, Figs. S1 and S2 of the supporting information.

## 2.3. COMSOL simulations

The 2D geometry of the reaction chamber was imported into COM-SOL to perform the simulations for obtaining the velocity, temperature, and concentration profiles of the reacting species [45,46]. The effect of temperature and flowrates (or residence time) on the final crystalline yield of HKUST-1 and uniformity of the deposition in the square chamber were studied. To account for the reaction between the two species, the activation energy and the pre-exponential factor obtained from the batch experiments were used in the Arrhenius equation to compute the rate constants. Navier Stokes equation was solved simultaneously with the continuity and energy balance equations to obtain the reaction and the temperature profiles. A typical physics-controlled mesh was utilized with the normal element size to perform these simulations. Further specific details of the computations are included in section S3 of the supporting information.

# 2.4. Microfluidic setup

Fig. 1(b) shows the exploded view of the microfluidic device consisting of three parts – reaction chamber, supporting mesh (membrane holder), and vacuum chamber. A 0.22  $\mu m$  nylon membrane is placed between the reaction chamber and the supporting mesh. The three parts (Fig. 1(b)) and the nylon membrane were assembled utilizing threaded screws and bolts. Fig. S1 shows the snapshot of the complete experimental setup for film deposition. The dimensions of the 3D printed parts and their drawings are described in section S2, Figs. S3 and S4 of the supporting information.

#### 2.5. MOF film synthesis procedure

The construction and working procedure for film deposition are as follows. The syringes were first filled with 15 mL of each precursor solution and wrapped with a silicon heating pad to attain the desired temperature (60–90  $^{\circ}$ C). The precursor solutions were then pumped through the microchannels at fixed flow rates (0.5–3 mL/min) to attain a desired concentration of reactants in the reaction chamber. The length and cross-section of the microchannel were adjusted to obtain the necessary residence time to achieve a 5-10% MOF yield. The prenucleated HKUST-1 crystals in the microchannel were then deposited in a square chamber where the reaction effluent came in contact with the nylon membrane. The continuous flow of the reaction mixture through the nylon membrane supported on a 3D printed mesh allows the growth of the deposited nuclei/crystals for the seamless formation of the film. After the desired period of deposition (2–20 min), the syringe pumps were switched off, and the vacuum pump was turned on to flush out the remaining reaction mixture in the microchannel and reaction chamber. The microfluidic device was disassembled, and the film was immersed in ethanol for 24 h in a glass bottle for dissolution of trapped precursors. Post this, the film was further dried under a vacuum at room temperature for 24 h.

The detailed experimental setup, CAD design, fabrication of the reactor-separator assembly, and operating procedures are included in sections S1, S2 and Figs. S3 and S4 of the supporting information.

# 2.6. Physical adherence test using sonication

The physical adherence of the HKUST-1 films on the nylon substrates were tested after complete drying of the fabricated films. The films were immersed in ethanol in a pyrex bottle and were placed in a Bransonic Ultrasonic bath for various periods of time. The films were taken, dried and SEM analysis were performed on all the films.

# 2.7. Characterization of HKUST films

The crystallinity of the thin films was confirmed using high-resolution XRD technique. The pore size distribution and BET surface areas of the deposited material were determined using  $N_2$  adsorption isotherms. The deposition and thickness of the films were analyzed using SEM and optical microscopy techniques. Specific instrumentation and characterization procedures for each of the mentioned techniques is included in section S2 of the supporting information.

# 2.8. CH<sub>4</sub>-H<sub>2</sub> gas separation experiments

Two identical cells with inlet and outlet channels were 3D printed inhouse. The fabricated films on nylon were sandwiched between the two cells. The side exposed to HKUST-1 film was the feed chamber and the other side exposed to bare nylon was the permeate chamber. This setup was fastened with screws and bolts to ensure no gas leaks, the edges were sealed with the help of the 3D printing resin and the setup was cured under UV light for 30 min. CH<sub>4</sub> and H<sub>2</sub>, 50% by volume each, were sent to the feed chamber at fixed flowrates and the carrier gas, Argon (Ar) was sent to the permeate chamber in a cross-current fashion. The separated gas mixture on the permeate side was fed to a gas chromatography system, where the concentration of each gas was measured. These experiments were performed for 1 h continuously and the data was recorded every 10 min. Control experiments with bare nylon were conducted to demonstrate the effect of HKUST-1 film on the separation factor of the gas mixture. Experimental details for the gas separation experiments are included in section S4 of the supporting information.

## 3. Results and discussion

In-situ FTIR experiments for batch syntheses were initially

performed to obtain the rate kinetics of HKUST-1 formation. The experimental setup and strategy were similar to the in-situ FTIR studies performed in previously published work, where rate kinetics of UIO-66 were computed and found to be in agreement with the Wide-Angle X-ray Scattering (WAXS) studies [38].

Fig. 2(a) shows the spectral signature of synthesized HKUST-1 in real-time, where the C=O peak at 1633 cm<sup>-1</sup>, C-O at 1370 cm<sup>-1</sup>, and the C-H out of plane bending at 729 cm<sup>-1</sup> are HKUST-1's molecular signatures [47,48]. Absorbance at the unique peak at 729 cm<sup>-1</sup> was chosen to be correlated with HKUST-1 formation to determine the yield in real time due to its reliable and reproducible intensities at specific product concentrations [47–49]. Calibration of the signal at 729 cm<sup>-1</sup> was performed with known concentrations of HKUST-1 (see Fig. S2). Fig. 2(b) shows the increase in intensity at 729 cm<sup>-1</sup> as a function of time during the reaction between the precursors (T = 60  $^{\circ}$ C). Using this calibration model, the crystalline yield was calculated at different time points during the synthesis, which was, in turn, studied at multiple temperatures, as shown in Fig. 2(c). The rate constants for each temperature were determined using the differential rate expression, compiled as the Arrhenius plot in Fig. 2(d). From this information, the overall activation energy was calculated to be 64.83 kJ/mol, which is in agreement with the previously published in-situ WAXS studies (~64-72 kJ/mol) [50]. Due to experimental limitations involving the ATR ZnSe crystal (elucidated in section S2, Fig. S5 of the supporting information), studies in the batch mode were performed only up to 60 °C. The activation energy obtained from these experiments was utilized to model reaction profiles and the product distribution in the reaction chamber (shown in Fig. 3) using COMSOL.

To design the continuous microfluidic reactor, a preliminary 3D model of the reactor was charted in Solidworks. A 2D version of this model was imported into COMSOL to setup Multiphysics simulations to gain further insights into the yields, velocity profiles and temperature

drops across the length of the reactor. A broad parameter range for flowrates (0.5-3 mL/min) and temperatures (60-100 °C) was used as the simulation space to understand the final product profiles, which facilitated the determination of an experimental design operation space for film deposition. The setup of the simulations is explained in detail in section S3 of the supporting information. The flow velocity profiles were first studied, as shown in Fig. 3(a), which helps us visualize patterns as the inlet of each precursor is set to 0.5 mL/min leading to an average flowrate of 1 mL/min. The gradient across the cross-section of the channel is due to the parabolic average velocity profile typically observed in laminar flows. Similar profiles were obtained across the range of all flowrates tested. To ensure that the reaction proceeds with significant yield, it was essential to understand the temperature drops across the length of the reactor. This was simulated by tweaking the channel length between 60 and 100 mm, where negligible temperature drops were observed across the channel length (Fig. 3(b)). This result assisted in eliminating irregular temperatures as a variable and reducing the model to account only for the most important variable, the residence time, to calculate yield. To study the HKUST-1 formation profile, the activation energy from the batch experiments was utilized by the Arrhenius expression in the Chemistry module to calculate rate constants at desired temperatures. These constants, coupled with temperature and flowrates used in the simulation, provided the crystalline yield profiles, as shown in Fig. 3(c). For the tested variable ranges, a yield between 5 and 10% was obtained at the exit of the channel, which opens to the square chamber. This observation is crucial because (1) it informed the mechanical design of the reactor, i.e., the length and diameter of the tubular channel; (2) it provided the uniform dispersion profile of the reaction effluent after it exited the tubular channel; and lastly (3) the effects of residence time in controlling the heterogeneous nucleation and growth on the porous substrate to some extent in the square chamber were assessed, which is discussed further later. The

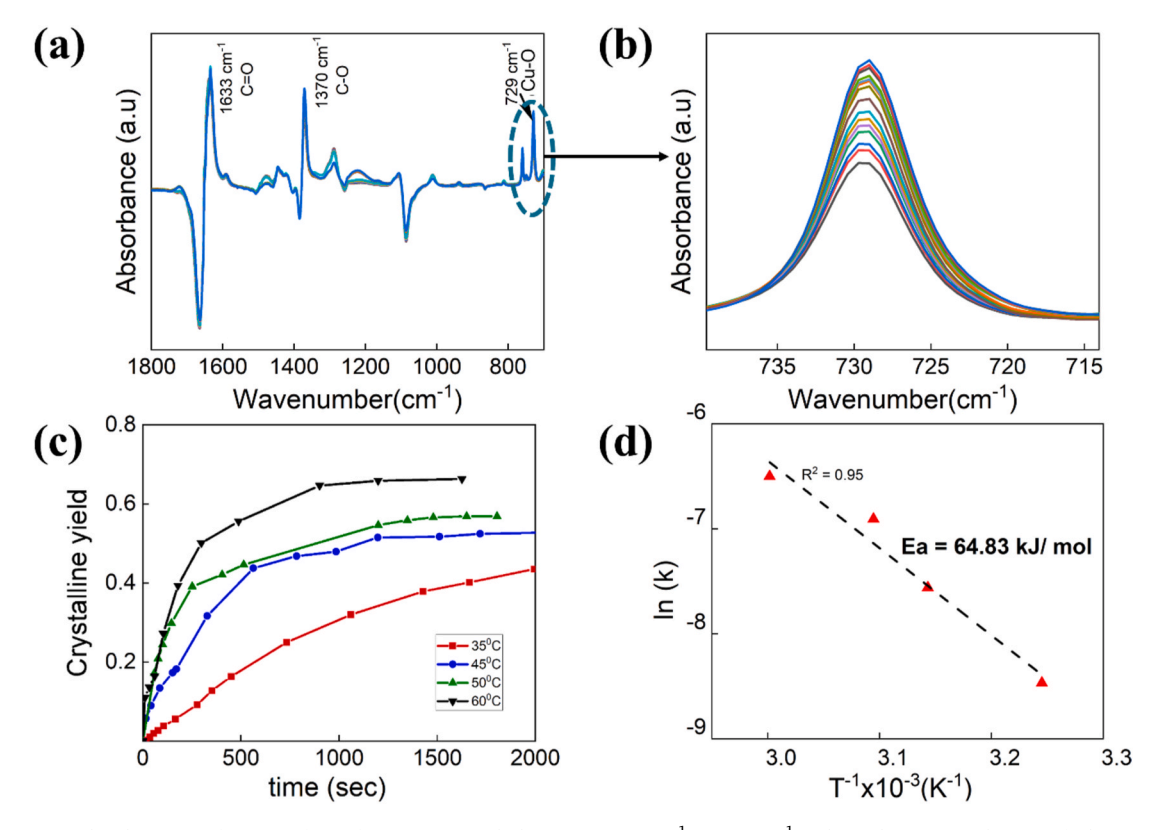


**Fig. 2.** (a) Increase in absorbance as a function of time for HKUST-1 peaks between 1800 cm<sup>-1</sup> to 650 cm<sup>-1</sup> in the mid-IR region. (b) Magnified view of the 729 cm<sup>-1</sup> signature peak of Cu–O bond in HKUST-1. The intensity increases as a function of time between 0 and 30 min. (c) Fractional crystalline yield vs. time obtained from batch in-situ FTIR experiments at varying temperatures. (d) Arrhenius plot obtained from rate constants at corresponding temperatures from batch experiments in (c). The obtained plot was extrapolated to predict the rate constants at higher temperatures further utilized in continuous tubular reactor design.

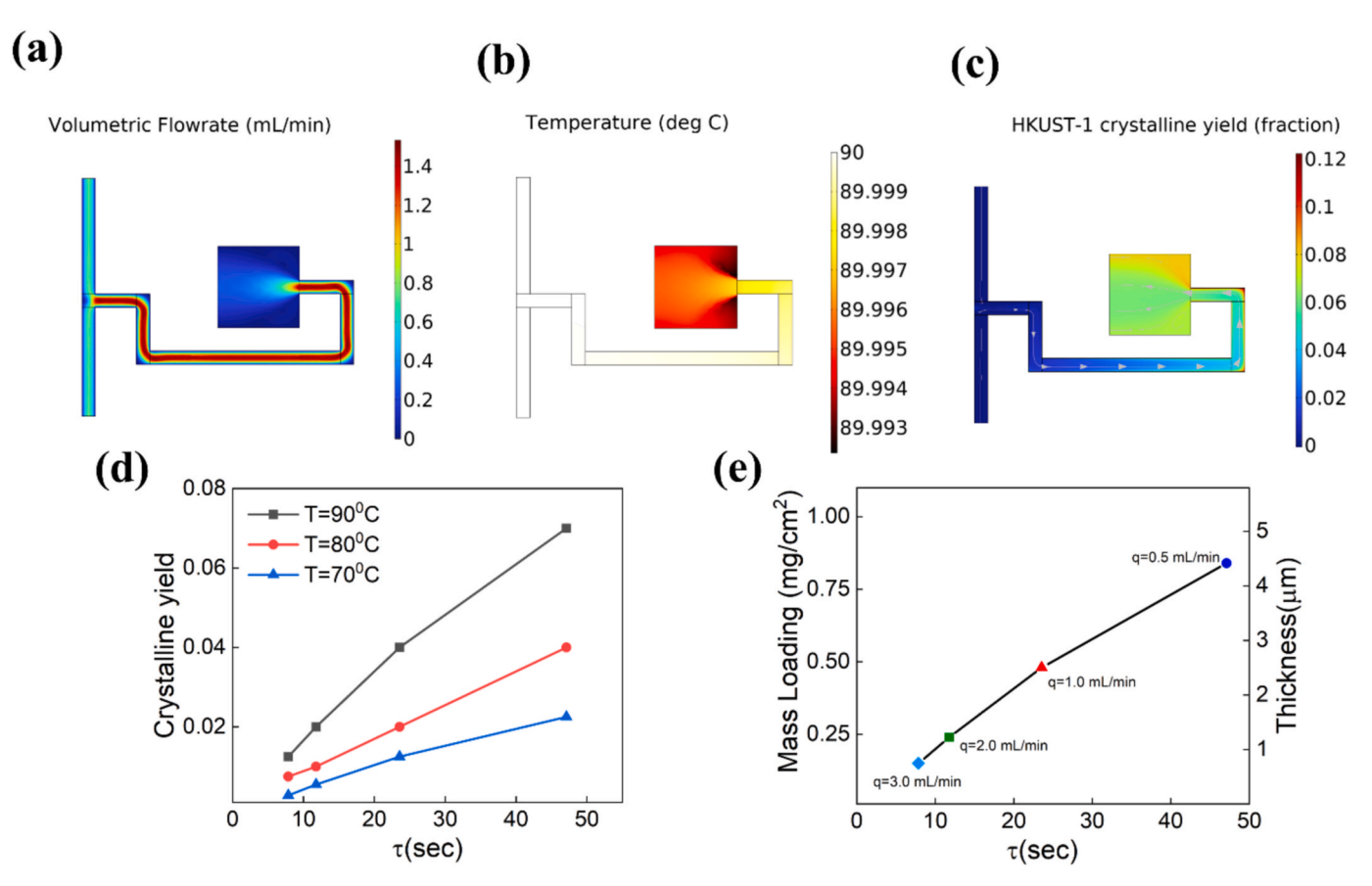


Fig. 3. COMSOL Multiphysics simulations to obtain different profiles across the length of the reaction channel at a flowrate of 1 mL/min (0.5 mL/min each precursor) and 90 °C inlet temperature of each precursor (a) Volumetric flowrate (mL/min) profile, (b) Temperature profile (OC), (c) HKUST-1 crystalline yield profile across the length of the channel, (d) HKUST-1 crystalline fraction predicted at different temperatures and residence times from COMSOL simulations. (e) Predicted mass loading and thickness of HKUST-1 films as a function of residence times with reaction temperature of 90 °C from COMSOL simulations. The length of the channels to obtain the results in this figure is set to 82 mm.

predicted final crystalline yields were obtained at various residence times for temperatures 70, 80, and 90  $^{\circ}$ C, as shown in Fig. 3(d). Significant crystalline yield is obtained at higher temperatures and longer residence times, due to which the temperature of the precursors was maintained at 90  $^{\circ}$ C during the experiments. As a best condition case, the mass loading and thickness of deposition across different residence times at this temperature were evaluated and graphed in Fig. 3(e). The final crystalline yield in the square chamber of the device was averaged in Fig. 3(d) and (e) due to the presence of a slight gradient, as seen in Fig. 3(c). These findings gave us strong insights into efficiently controlling the loading and thickness of the films while conducting the experiments.

Furthermore, based on the mechanical design parameters obtained from COMSOL simulations, a 3D model of the device was fabricated (section S2 and Fig. S1 of the supporting information. HKUST-1 was deposited on nylon substrates at 90 °C by the coupled percolationsecondary growth mechanism. The residence and processing times were varied to obtain a range of mass loadings and thicknesses. Highresolution XRD and BET measurements (Fig. 4(a) and (b)) confirmed crystallinity and the pore size distributions of HKUST-1 deposition. The BET surface area of particles was obtained to be 1493 m<sup>2</sup>/g, which is equivalent to the previously reported values via the microwave approach for HKUST-1 film synthesis [51]. The N2 adsorption isotherm obtained is included in the supporting information (Fig. S6). Fig. 4(c) shows the comparison of the theoretically predicted and experimentally obtained mass loading as a function of processing time. Film thicknesses were measured using optical microscopy, in which the portions of the films were mounted on vertical scanning electron microscopy (SEM)

stubs for measurements. Thickness measurements of a few samples were performed under SEM and were in good agreement with that obtained from optical microscopy, as shown in Fig. 4(d) and (e). Details of the instruments and characterization procedure for optical microscope and SEM are included in section S2 of the supporting information. Fig. 4(f) shows the comparison of the theoretically predicted and experimental film thicknesses with an increase in time. The deviation of the quantitative aspects of the experimentally fabricated films (seen in Fig. 4(c) and (f)) from the theoretical predictions can be attributed to the interfacial growth of crystals that occur due to the heterogeneous nucleation on the binding substrate.

Since a quantitative parameter to model for the heterogeneous nucleation cannot be included in the Multiphysics model, experimentally controlling the flowrates and passage of the reactant effluent through the porous substrate allowed its control to some extent. Due to the lack of a significant pressure gradient across the porous membrane, the reaction effluent would easily pass through during the initial time stamps, leaving the crystals onto the substrate. However, with increasing yield, a fair amount of the reaction mixture accumulates inside the square chamber (approximately 30-40% by volume), and the remaining seeps through the membrane due to crystals blocking the flow path. The quantity of deposited crystals can be controlled per unit time by controlling the residence time in these situations. Thus, operating at low residence times (high flowrates) results in maximum removal of the reaction effluent, minimizing the heterogeneous growth on the substrate if desired. However, in the best interest of obtaining well-adhered and contiguous films, heterogeneous growth, to some extent, is desirable. Compared to films fabricated at low residence times, significant

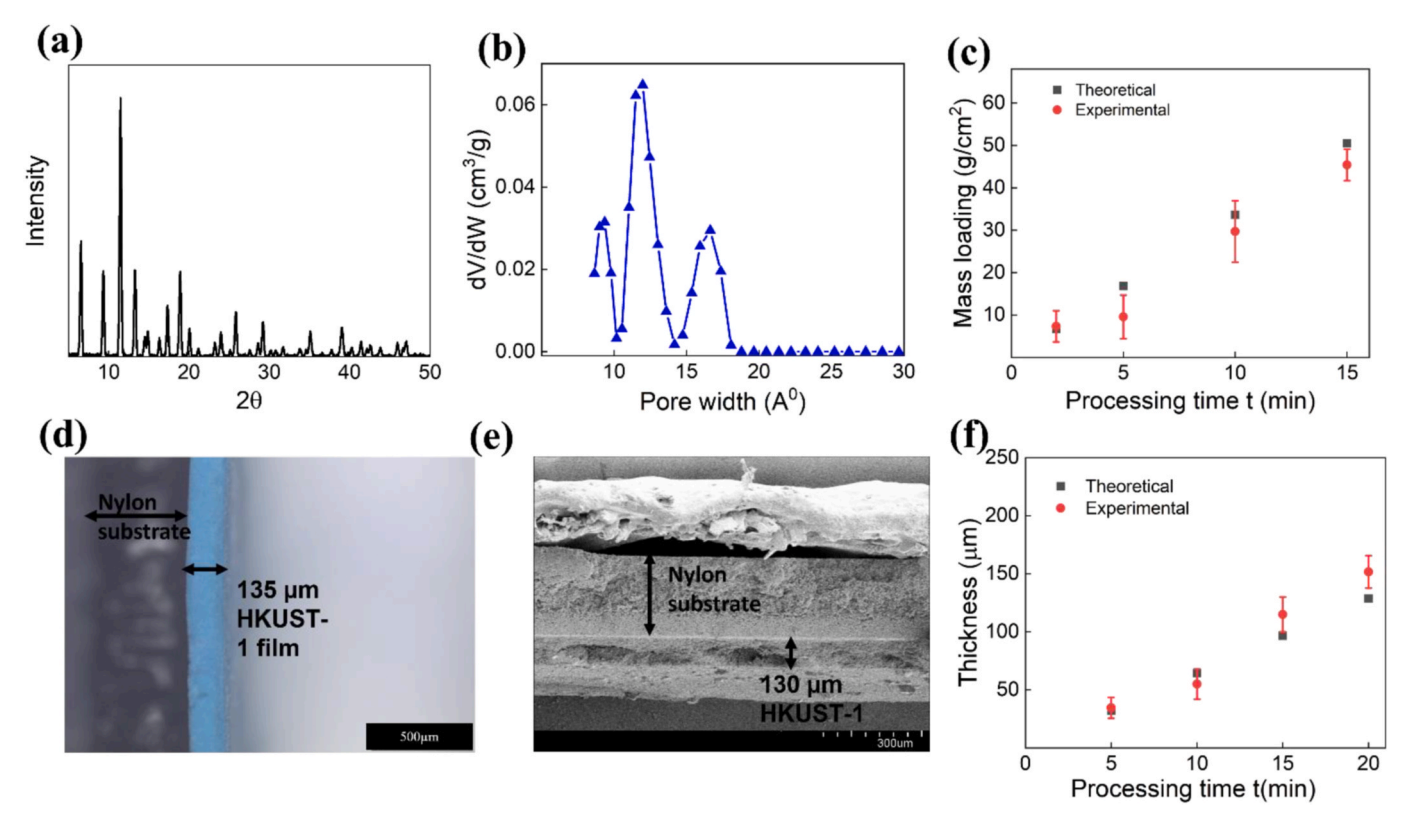


Fig. 4. (a) Powder-XRD spectra of HKUST-1 film on a nylon substrate. (b) Pore size distribution of the HKUST-1 powder deposition obtained from BET measurements- $N_2$  adsorption isotherm. (c) Theoretically predicted and experimentally obtained mass loadings of HKUST-1 films vs. processing times at  $T=90\,^{\circ}C$  and fixed residence time of 24 s (fixed operating flowrate = 1 mL/min). (d) Cross-sectional view of the HKUST-1 film under an optical microscope, obtained after 20 min of processing at  $T=90\,^{\circ}C$  and fixed residence time of 24 s (fixed operating flowrate = 1 mL/min). (e) The cross-section view of the same HKUST-1 film as in (d) was obtained from SEM imaging. (f) Theoretically predicted and experimentally obtained thicknesses of HKUST-1 films vs. processing times at  $T=90\,^{\circ}C$  and fixed residence time of 24 s (fixed operating flowrate = 1 mL/min).

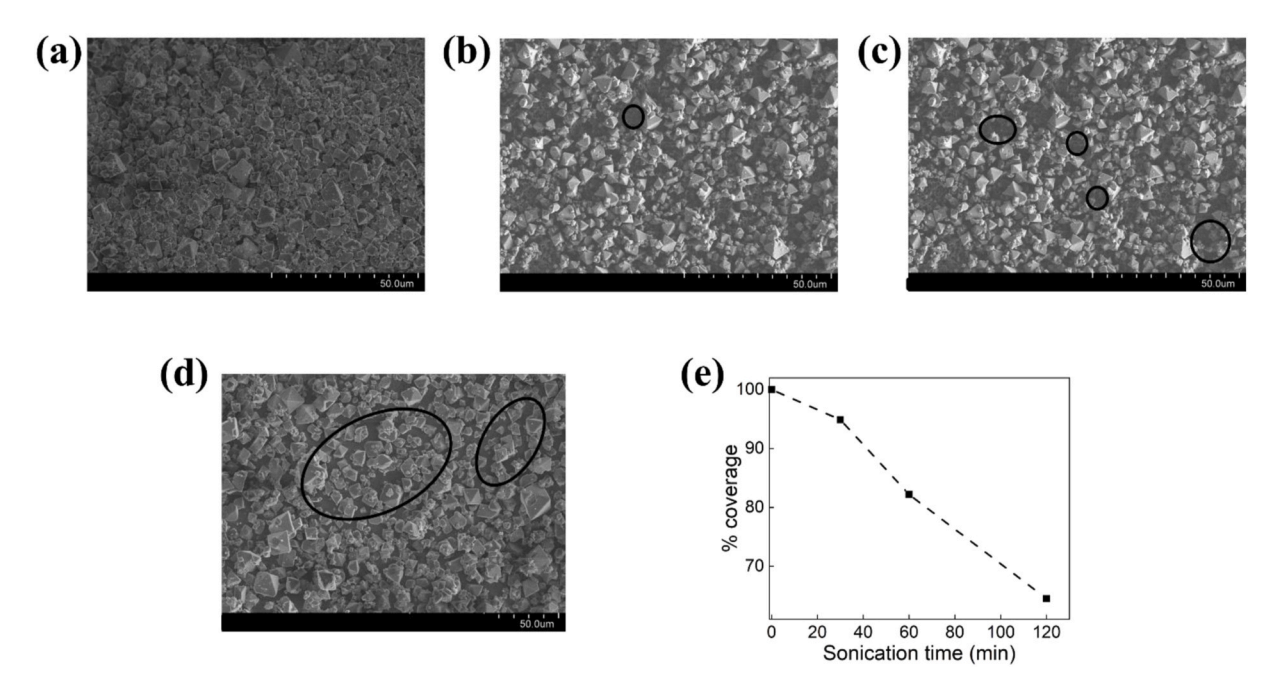


Fig. 5. (a) SEM image of a vacuum-dried film before sonication, SEM image of dried films after (b) 30 min sonication, (c) 60 min, and (d) 120 min. (e) % coverage vs. sonication time. The individual films in (a) to (d) were fabricated at 1 mL/min flowrate and 90 °C. The thickness of the films for sonication experiments were  $\sim$ 25  $\mu$ m.

differences in the adherence to these substrates were observed. The physical stability of the film on the substrates was tested by the sonication method, which has been used before to demonstrate the stability of MOF films subjected to harsh conditions [52].

A set of films were synthesized to test the physical adhesion with a flowrate of 1 mL/min for 10 min, vacuum dried for 24 h, and immersed in ethanol. Sonication was performed for 30, 60, and 120 min on separate films. Following this step, the films were vacuum dried for 24 h. The surface coverage and orientation of HKUST-1 crystals were studied by SEM and further analyzed in ImageJ to obtain the coverage values to demonstrate the strong physical adhesion obtained using the PAC technique. Fig. 5 (a)-(d) shows the SEM images of the deposited crystals. It was seen that after 30 min, more than 95% of the deposited crystals remained intact on the surface without any change in the thickness of the film (observed under an optical microscope). Voids started to appear in the deposition after 60 min with  $\sim$ 80% of the crystals intact, which further reduced to 60% intact crystal after 120 min. The percentage coverage vs. sonication time is shown in Fig. 5(e). Films of similar thickness and loading were fabricated at higher flowrates, i.e., 2.5-3 mL/min and subjected to sonication for the physical adherence test. It was observed that % coverage slightly dropped compared to the films that were fabricated at 1 mL/min. This implies that the reaction effluent in the square chamber promotes inter-grain growth on the substrate, enhancing the packing and conformity of the deposited films with uni-

Along with the strong adherence to the substrate, minimizing the inter-grain boundaries or, in other words, cracking is essential. This phenomenon is more prominent in deposition on porous substrates than

on solid substrates. It was worth noting that when the films were dried at high temperatures in a conventional oven, significant cracks between the films were observed compared to the vacuum-dried films. Therefore, this post-processing step is equally crucial to preserve the synthesized films' physical stability. Ultimately, the films displayed strong adherence and intact coverage post sonication, proving that the films can withstand high-pressure environments. More SEM images (top and cross-sectional view) are included in Fig. S7 of the supporting information.

To prove the wide applicability and robustness of the developed technique, MOF-505 films were also fabricated (SEM image shown in Fig.S8 of the supporting information), where a previously reported batch synthesis for MOF-505 was adopted to fabricate these films continuously [53].

These materials were finally deployed for the separation of CH<sub>4</sub> and H<sub>2</sub> gas mixture to benchmark the performance of the films and the fabrication mechanism. The separation experiments were designed such that the gas mixture enters the upstream at a flowrate of 200 standard cm³/min (SCCM), each at 50% by volume (100 SCCM H<sub>2</sub> + 100 SCCM CH<sub>4</sub>). Downstream of the separation process, the gas was mixed with Argon (Ar) (the carrier gas) which was then sent to a gas chromatography system to determine the concentration of separated species. Fig. 5 (a) shows the schematic of these experiments. The carrier gas Ar is flown in a counter-current fashion. The device housing the membrane for these experiments was fabricated in-house (Fig. 6(b)). As shown in this figure, the setup is assembled as discussed previously in the main manuscript (section 2.6) and the supporting information (section S4 and Fig. S9).

Fig. 6(c) shows the concentration of H<sub>2</sub> and CH<sub>4</sub> gas with a blank

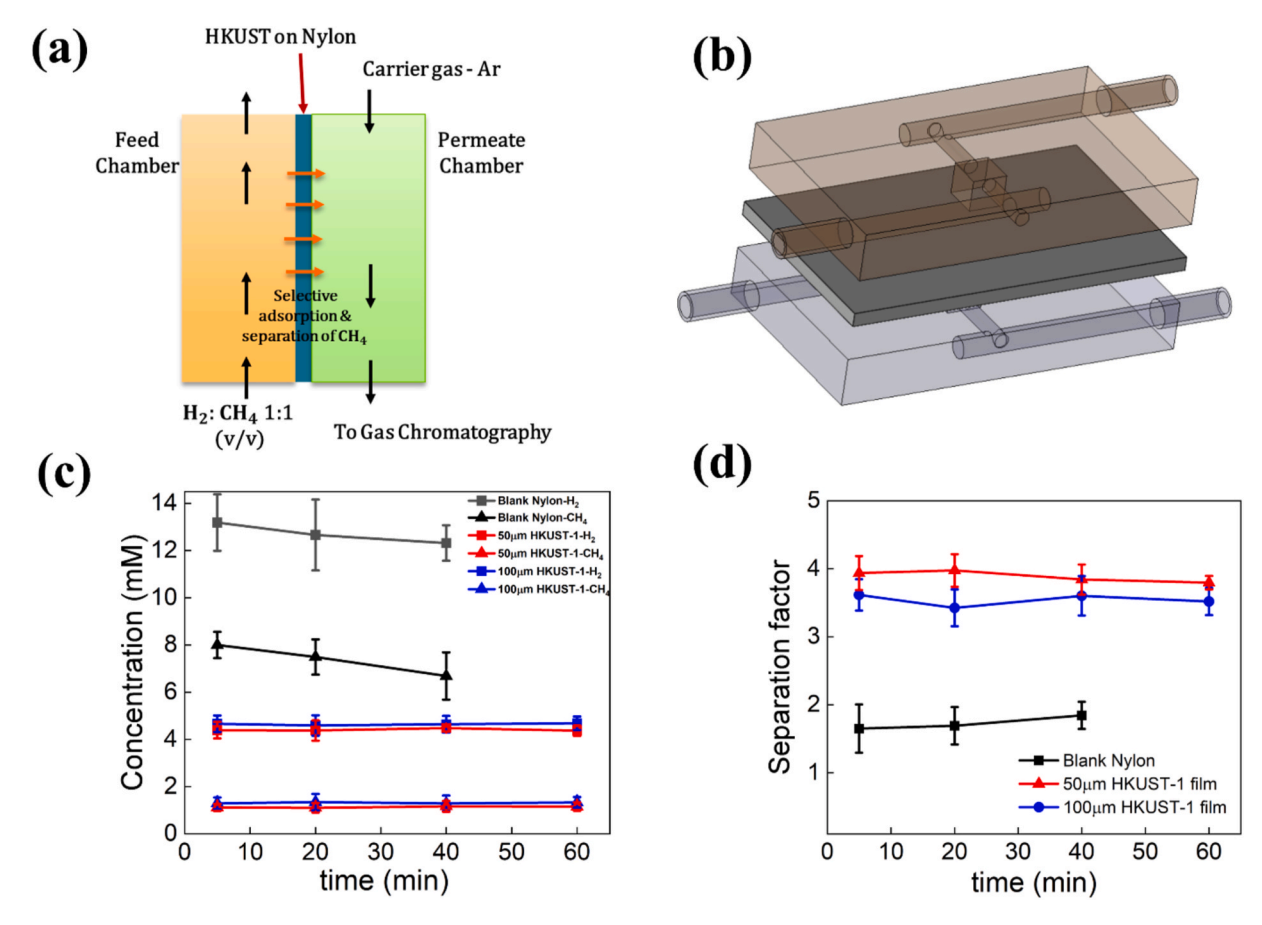


Fig. 6. (a) Schematic of  $CH_4/H_2$  separation using HKUST-1 membranes. The feed stream flowrate is 200 SCCM (100 SCCM  $CH_4$  and 100 SCCM  $H_2$ ), and Argon (Ar) is used as carrier gas on the permeate side. Ar is passed at 200 SCCM flowrate on the permeate side that carries certain amounts of  $CH_4$  and  $H_2$  through the membrane sent to Gas chromatography to determine the concentration of each gas, (b) 3D design isometric view of the device that is used for separation experiments. The HKUST-1 deposited on nylon is sandwiched between the two 3d printed feed and permeate chambers, (c) Concentration of  $H_2$  and  $CH_4$  gases on the permeate side from GC vs. time (for a single run), (d) Separation factor for blank nylon and HKUST-1 film of different thicknesses as a function of time.

nylon membrane, with 50  $\mu$ m and 100  $\mu$ m HKUST-1 deposition on nylon. The concentration of each of the gases on the upstream/feed side was 20 mM (considering 100 SCCM flowrate of each gas). With no deposition, about 70% of the H<sub>2</sub> and less than 50% of CH<sub>4</sub> were detected on the permeate side. However, with HKUST-1 deposited films, the concentration of CH<sub>4</sub> on the permeate side drops significantly, implying that HKUST-1 adsorbs the majority of CH<sub>4</sub>. The concentration of H<sub>2</sub> also dropped; however, the separation gap between the two gases was observed to increase, thus showing a high selectivity of HKUST-1 towards CH<sub>4</sub>. The permeability values of H<sub>2</sub> and CH<sub>4</sub> were 4.85 x  $10^{-6}$  mol m<sup>-2</sup> s<sup>-1</sup>.Pa<sup>-1</sup> and 1.25 x  $10^{-6}$  mol m<sup>-2</sup> s<sup>-1</sup>.Pa<sup>-1</sup> respectively which are in agreement with the previously reported separation experiments for this mixture [54–57]. Based on the obtained permeabilities, the separation factors were calculated using the following equation:

Separation factor = 
$$\frac{\text{Permeability of H}_2(\textit{mol.m}^{-2}\textit{s}^{-1}\textit{Pa}^{-1})}{\text{Permeability of CH}_4(\textit{mol.m}^{-2}\textit{s}^{-1}\textit{Pa}^{-1})}$$

Fig. 6(d) shows the steady separation factor of 4.3 with a 50 and 100 μm thick HKUST-1 deposition. Negligible changes in the separation factors were observed as a function of film thickness. This suggests that the selectivity of CH<sub>4</sub> on HKUST-1 has a very slight dependence on the film thickness. The obtained values are not only in agreement with the previous experimental efforts [54,57], but also with theoretical values of the separation factor for H<sub>2</sub>/CH<sub>4</sub> mixture. The Knudsen separation factor which is the ratio of the diffusion fluxes of both the gases, states that the diffusion fluxes are inversely proportional to the square root molar masses of the gas. Based on that, we obtain 2.82 as the separation factor for this mixture. The gas separation experiments were also performed on films that did not have complete coverage and the separation factors were observed to drop. Thus, a uniform and contiguous deposition is a prime aspect of ensuring the effective separation of this gas mixture. Long term experiments upto 12h were performed to display the stability of the separation which is included in Fig. S10 of the supporting information. This would also be important for other gas mixtures that can be effectively separated using HKUST-1 films.

To accelerate the fabrication and screening of these films, a reaction chamber consisting of four deposition chambers was designed, as shown in Fig. S11, that can be used to fabricate multiple films in a single run inspired by previous studies for active pharmaceutical ingredient (API) screening. Flow distributors [46] can be utilized instead of multiple pumps to vary the residence times of the precursors entering the different chambers. This would yield films of different thicknesses and loadings as desired with very short processing times.

## 4. Conclusion

This work presents an inexpensive, reliable, and scalable PAC approach to fabricating robust HKUST-1 films with the development and use of a well-controlled continuous microfluidic device that helps finetune the quantitative and qualitative aspects of the films. Optimizing the deposition mechanism, i.e., percolation coupled with controlled heterogeneous nucleation and growth, ensures film contiguity and strong adherence to the substrate. The fabricated HKUST-1 films perform well in separating the  $\mathrm{CH_4-H_2}$  binary mixture with reproducible and steady separation factors. These films can be easily adapted to other applications like electrocatalysis by enhancing their conductivity by simply soaking them in conductive solutions like Nafion, TCNQ, etc. [37] This technique can be adapted to various porous substrates like PVDF, PTFE, carbon paper, etc., while offering flexibility to make substrate modifications before assembling the devices, making it applicable for a wide range of multifaceted depositions.

In summary, kinetic data obtained from the batch was utilized to develop a COMSOL Multiphysics model, which provided necessary insight into the design and operational parameters for experimentation. This straightforward protocol can be easily deployed in fabricating a

wide range of MOF and COF films with effective kinetic formation rates. To prove the wide applicability and robustness of PAC method, MOF-505 films were fabricated using continuous microfluidic reactor. Based on the rate kinetics of a given MOF/COF, film formation with effective deposition can easily be achieved with this method by varying temperature and residence time variables. The control of the operating parameters to obtain desired thickness and loading makes the PAC process a potential candidate for scaling up the film fabrication processes.

#### Author statement

Rajan R. Bhawnani: Methodology, Data curation, Writing- Original draft preparation, Visualization, Investigation, Formal Analysis, Rohan Sartape: Investigation, Formal Analysis, Writing- Reviewing and Editing, Aditya Prajapati: Investigation, Formal Analysis, Writing- Reviewing and Editing, Prem K.R. Podupu: Investigation, Formal Analysis, Writing- Reviewing and Editing, Paria Coliaie: Methodology, Investigation, Formal Analysis, Writing- Reviewing and Editing, Arnav N. Nere: Investigation, Formal Analysis, Writing- Reviewing and Editing, Meenesh R Singh: Conceptualization, Supervision, Writing- Reviewing and Editing, Resources, Funding Acquisition.

# Declaration of competing interest

The authors declare the following financial interests/personal relationships which may be considered as potential competing interests:

Meenesh R. Singh has patent #UIC-2023-026: PERCOLATION-ASSISTED COATING OF METAL-ORGANIC FRAMEWORKS ON POROUS pending to The Board of Trustees of the University of Illinois.

# Data availability

Data will be made available on request.

# Acknowledgements

This material is based on the work performed at the Materials and Systems Engineering Laboratory (MaSEL) at the University of Illinois at Chicago (UIC). M.R.S. acknowledges funding support from UIC and the US National Science Foundation (NSF, EFRI 2132022). This work made use of the NCF facilities at UIC for XRD measurements This work also made use of the EPIC facility of Northwestern University's NUANCE Center for SEM measurements, which has received support from the SHyNE Resource (NSF ECCS-2025633), the IIN, and Northwestern's MRSEC program (NSF DMR-1720139). The authors would like to acknowledge Benjamin Shindel (Dravid group) and Neil Schweitzer (REACT facilities) at Northwestern University for assisting with BET measurements. We would like to thank Nishithan C. Kani (MaSEL, Chemical Engineering, UIC) for useful discussions on gas separation presented in this work. R.R.B. would like to thank Prof. Nita Mehta and Dr. Vipul Shah for constant inspiration in the aspects of polymer chemistry and reactor design.

## Appendix A. Supplementary data

Supplementary data to this article can be found online at  $\frac{\text{https:}}{\text{doi.}}$  org/10.1016/j.memsci.2022.121202.

# References

- [1] H.-C. Zhou, J.R. Long, O.M. Yaghi, ACS Publications, vol. 112, 2012, pp. 673-674.
- [2] H. Furukawa, K.E. Cordova, M. O'Keeffe, O.M. Yaghi, The chemistry and applications of metal-organic frameworks, Science 341 (2013), 1230444.
- [3] Y. Deng, et al., Metal-organic framework membranes: recent development in the synthesis strategies and their application in oil-water separation, Chem. Eng. J. 405 (2021), 127004.

- [4] C. Crivello, et al., Advanced technologies for the fabrication of MOF thin films, Mater. Horiz. 8 (2021) 168–178.
- [5] M.M. Mohseni, et al., Metal-organic frameworks (MOF) based heat transfer: a comprehensive review, Chem. Eng. J. (2022), 137700.
- [6] N. Rabiee, et al., Bioactive hybrid metal-organic framework (MOF)-based nanosensors for optical detection of recombinant SARS-CoV-2 spike antigen, Sci. Total Environ. 825 (2022), 153902.
- [7] N. Rabiee, et al., Green metal-organic frameworks (MOFs) for biomedical applications, Microporous Mesoporous Mater. (2022), 111670.
- [8] A. Sultana, A. Kathuria, K.K. Gaikwad, Metal-organic frameworks for active food packaging. A review, Environ. Chem. Lett. (2022) 1–17.
- [9] K. Ikigaki, K. Okada, M. Takahashi, Epitaxial growth of multilayered metal-organic framework thin films for electronic and photonic applications, ACS Appl. Nano Mater. 4 (2021) 3467–3475.
- [10] O. Shekhah, J. Liu, R. Fischer, C. Wöll, MOF thin films: existing and future applications, Chem. Soc. Rev. 40 (2011) 1081–1106.
- [11] L. Abdul Ghani, N.a. Ali, I.S. Nazaran, M.M. Hanafiah, Environmental performance of small-scale seawater reverse osmosis plant for rural area water supply, Membranes 11 (2021) 40.
- [12] C. Zhou, et al., Metal organic frameworks (MOFs) as multifunctional nanoplatform for anticorrosion surfaces and coatings, Adv. Colloid Interface Sci. (2022), 102707.
- [13] L. Jiang, et al., Recent advances of metal-organic frameworks in corrosion protection: from synthesis to applications, Chem. Eng. J. 430 (2022), 132823.
- [14] H. Zhang, et al., Ultrafast selective transport of alkali metal ions in metal organic frameworks with subnanometer pores, Sci. Adv. 4 (2018), eaaq0066.
- [15] K.A. Stults, Metal Organic Framework-Metal Oxide Composites for Toxic Gas Adsorption and Sensing, GEORGIA TECH RESEARCH CORP ATLANTA, 2014.
- [16] G. Rim, et al., Sub-ambient temperature direct air capture of CO2 using amineimpregnated MIL-101 (Cr) enables ambient temperature CO2 recovery, JACS Au 2 (2022) 380–393.
- [17] B. Min, et al., Continuous zeolite MFI membranes fabricated from 2D MFI nanosheets on ceramic hollow fibers, Angew. Chem. Int. Ed. 58 (2019) 8201–8205.
- [18] S. Qiu, M. Xue, G. Zhu, Metal-organic framework membranes: from synthesis to separation application, Chem. Soc. Rev. 43 (2014) 6116–6140.
- [19] S.E. Henkelis, S.J. Percival, L.J. Small, D.X. Rademacher, T.M. Nenoff, Continuous MOF membrane-based sensors via functionalization of interdigitated electrodes, Membranes 11 (2021) 176.
- [20] F. Seidi, et al., Metal-organic framework (MOF)/epoxy coatings: a review, Materials 13 (2020) 2881.
- [21] Y. Hu, et al., Zeolitic imidazolate framework/graphene oxide hybrid nanosheets as seeds for the growth of ultrathin molecular sieving membranes, Angew. Chem. 128 (2016) 2088–2092.
- [22] K.R. Tulig, Encapsulation of Nanoparticles in Metal-Organic Frameworks for Air Purification, Georgia Institute of Technology, 2016.
- [23] C. Crivello, et al., Advanced technologies for the fabrication of MOF thin films, Mater. Horiz. 8 (2021) 168–178.
- [24] Y. He, et al., Incorporating metal-organic frameworks into substrates for environmental applications, Chem. Eng. J. (2022), 136866.
- [25] F. Al-Ghazzawi, L. Conte, C. Richardson, P. Wagner, Reactive extrusion printing for simultaneous crystallization-deposition of metal-organic framework films, Angew. Chem. Int. Ed. 61 (2022), e202117240.
- [26] S. Hermes, F. Schröder, R. Chelmowski, C. Wöll, R.A. Fischer, Selective nucleation and growth of metal- organic open framework thin films on patterned COOH/CF3terminated self-assembled monolayers on Au (111), J. Am. Chem. Soc. 127 (2005) 13744–13745
- [27] M.C. So, et al., Layer-by-layer fabrication of oriented porous thin films based on porphyrin-containing metal-organic frameworks, J. Am. Chem. Soc. 135 (2013) 15698–15701
- [28] Q. Zhang, Y. Pramudya, W. Wenzel, C. Wöll, Modeling the layer-by-layer growth of HKUST-1 metal-organic framework thin films, Nanomaterials 11 (2021) 1631.
- [29] C.-W. Kung, et al., Post metalation of solvothermally grown electroactive porphyrin metal-organic framework thin films, Chem. Commun. 51 (2015) 2414–2417.
- [30] O. Shekhah, et al., Layer-by-layer growth of oriented metal organic polymers on a functionalized organic surface, Langmuir 23 (2007) 7440–7442.
- [31] J. Liu, C. Wöll, Surface-supported metal-organic framework thin films: fabrication methods, applications, and challenges, Chem. Soc. Rev. 46 (2017) 5730–5770.
- [32] V. Chernikova, O. Shekhah, M. Eddaoudi, Advanced fabrication method for the preparation of MOF thin films: liquid-phase epitaxy approach meets spin coating method, ACS Appl. Mater. Interfaces 8 (2016) 20459–20464.

- [33] X.-j. Bai, et al., Fabrication of MOF thin films at miscible liquid-liquid interface by spray method, ACS Appl. Mater. Interfaces 10 (2018) 25960–25966.
- [34] Q. Qian, et al., MOF-based membranes for gas separations, Chem. Rev. 120 (2020) 8161–8266.
- [35] A.J. Brown, et al., Interfacial microfluidic processing of metal-organic framework hollow fiber membranes, Science 345 (2014) 72–75.
- [36] S. Guthrie, et al., Crystallization of high aspect ratio HKUST-1 thin films in nanoconfined channels for selective small molecule uptake, Nanoscale Adv. 1 (2019) 2946–2952.
- [37] S. Jung, L. Huelsenbeck, Q. Hu, S. Robinson, G. Giri, Conductive, large-area, and continuous 7, 7, 8, 8-Tetracyanoquinodimethane@ HKUST-1 thin films fabricated using solution shearing, ACS Appl. Mater. Interfaces 13 (2021) 10202–10209.
- [38] A.V. Dighe, et al., Autocatalysis and oriented attachment direct the synthesis of a metal-organic framework, JACS Au 2 (2022) 453–462.
- [39] A. Ghorbanpour, L.D. Huelsenbeck, D.-M. Smilgies, G. Giri, Oriented UiO-66 thin films through solution shearing, CrystEngComm 20 (2018) 294–300.
- [40] J.-C. Lee, J.-O. Kim, H.-J. Lee, B. Shin, S. Park, Meniscus-guided control of supersaturation for the crystallization of high quality metal organic framework thin films, Chem. Mater. 31 (2019) 7377–7385.
- [41] J.-O. Kim, et al., Large-area synthesis of nanoscopic catalyst-decorated conductive MOF film using microfluidic-based solution shearing, Nat. Commun. 12 (2021) 1–8.
- [42] D. Nagaraju, D.G. Bhagat, R. Banerjee, U.K. Kharul, In situ growth of metal-organic frameworks on a porous ultrafiltration membrane for gas separation, J. Mater. Chem. 1 (2013) 8828–8835.
- [43] M. Faustini, et al., Microfluidic approach toward continuous and ultrafast synthesis of metal-organic framework crystals and hetero structures in confined microdroplets, J. Am. Chem. Soc. 135 (2013) 14619–14626.
- [44] A.M. Marti, S.R. Venna, E.A. Roth, J.T. Culp, D.P. Hopkinson, Simple fabrication method for mixed matrix membranes with in situ MOF growth for gas separation, ACS Appl. Mater. Interfaces 10 (2018) 24784–24790.
- [45] P. Coliaie, et al., On-the-spot quenching for effective implementation of cooling crystallization in a continuous-flow microfluidic device, React. Chem. Eng. 7 (2022) 1179–1190.
- [46] P. Coliaie, et al., Advanced continuous-flow microfluidic device for parallel screening of crystal polymorphs, morphology, and kinetics at controlled supersaturation, Lab Chip 21 (2021) 2333–2342.
- [47] R. Lin, L. Ge, H. Diao, V. Rudolph, Z. Zhu, Ionic liquids as the MOFs/polymer interfacial binder for efficient membrane separation, ACS Appl. Mater. Interfaces 8 (2016) 32041–32049.
- [48] N.R. Dhumal, M.P. Singh, J.A. Anderson, J. Kiefer, H.J. Kim, Molecular interactions of a Cu-based metal-organic framework with a confined imidazolium-based ionic liquid: a combined density functional theory and experimental vibrational spectroscopy study, J. Phys. Chem. C 120 (2016) 3295–3304.
- [49] M.J. Lis, et al., In-situ direct synthesis of HKUST-1 in wool fabric for the improvement of antibacterial properties, Polymers 11 (2019) 713.
- [50] M.J. Van Vleet, T. Weng, X. Li, Schmidt, J. In situ, time-resolved, and mechanistic studies of metal-organic framework nucleation and growth, Chem. Rev. 118 (2018) 3681–3721.
- [51] C. McKinstry, E.J. Cussen, A.J. Fletcher, S.V. Patwardhan, J. Sefcik, Scalable continuous production of high quality HKUST-1 via conventional and microwave heating, Chem. Eng. J. 326 (2017) 570–577.
- [52] A. Mähringer, J.M. Rotter, D.D. Medina, Nanostructured and oriented metalorganic framework films enabling extreme surface wetting properties, Beilstein J. Nanotechnol. 10 (2019) 1994–2003.
- [53] Y. Chen, et al., A new MOF-505@ GO composite with high selectivity for CO2/CH4 and CO2/N2 separation, Chem. Eng. J. 308 (2017) 1065–1072.
- [54] Y. Mao, et al., Pressure-assisted synthesis of HKUST-1 thin film on polymer hollow fiber at room temperature toward gas separation, ACS Appl. Mater. Interfaces 6 (2014) 4473–4479.
- [55] V.V. Guerrero, Y. Yoo, M.C. McCarthy, H.-K. Jeong, HKUST-1 membranes on porous supports using secondary growth, J. Mater. Chem. 20 (2010) 3938–3943.
- [56] Q. Yang, et al., Exceptional high selectivity of hydrogen/methane separation on a phosphonate-based MOF membrane with exclusion of methane molecules, Chem. Commun. 53 (2017) 9797–9800.
- [57] H. Guo, G. Zhu, I.J. Hewitt, S. Qiu, Twin copper source" growth of metal- organic framework membrane: Cu3 (BTC) 2 with high permeability and selectivity for recycling H2, J. Am. Chem. Soc. 131 (2009) 1646–1647.